minerals

MDPI

Article

Enhanced Potential Toxic Metal Removal Using a Novel Hierarchical SiO_2–$Mg(OH)_2$ Nanocomposite Derived from Sepiolite

Qi-Zhi Yao [1], Sheng-Hui Yu [2,3,*], Tian-Lei Zhao [2,4], Fei-Jin Qian [2,4], Han Li [2,4], Gen-Tao Zhou [2,4,*] and Sheng-Quan Fu [5]

1 School of Chemistry and Materials Science, University of Science and Technology of China, Hefei 230026, China; qzyao@ustc.edu.cn
2 CAS Key Laboratory of Crust-Mantle Materials and Environments, School of Earth and Space Sciences, University of Science and Technology of China, Hefei 230026, China; zhaotian@mail.ustc.edu.cn (T.-L.Z.); fjqian@mail.ustc.edu.cn (F.-J.Q.); lihan211@mail.ustc.edu.cn (H.L.)
3 School of Environmental Science and Engineering, Shaanxi University of Science and Technology, Xi'an 710021, China
4 CAS Center for Excellence in Comparative Planetology, Hefei 230026, China
5 Hefei National Laboratory for Physical Sciences at Microscale, University of Science and Technology of China, Hefei 230026, China; fusq@ustc.edu.cn
* Correspondence: yushenghui@sust.edu.cn (S.-H.Y.); gtzhou@ustc.edu.cn (G.-T.Z.)

Received: 9 April 2019; Accepted: 14 May 2019; Published: 15 May 2019

Abstract: Clays are widely used as sorbents for heavy metals due to their high specific surface areas, low cost, and ubiquitous occurrence in most soil and sediment environments. However, the low loading capacity for heavy metals is one of their inherent limitations. In this work, a novel SiO_2–$Mg(OH)_2$ nanocomposite was successfully prepared via sequential acid–base modification of raw sepiolite. The structural characteristics of the resulting modified samples were characterized by a wide range of techniques including field emission scanning electron microscopy (FESEM), transmission electron microscopy (TEM), energy dispersive X-ray spectroscopy (EDX), X-ray diffraction (XRD), and nitrogen physisorption analysis. The results show that a hierarchical nanocomposite constructed by loading the $Mg(OH)_2$ nanosheets onto amorphous SiO_2 nanotubes can be successfully prepared, and the nanocomposite has a high surface area (377.3 m^2/g) and pore volume (0.96 cm^3/g). Batch removal experiments indicate that the nanocomposite exhibits high removal efficiency toward Gd(III), Pb(II), and Cd(II), and their removal capacities were greatly enhanced in comparison with raw sepiolite, due to the synergistic effect of the different components in the hierarchical nanocomposite. This work can provide a novel route toward a hierarchical nanocomposite by using clay minerals as raw material. Taking into account the simplicity of the fabrication route and the high loading capacities for heavy metals, the developed nanocomposite also has great potential applications in water treatment.

Keywords: hierarchical nanocomposite; sepiolite; clay mineral; heavy metals; water treatment

1. Introduction

Heavy metals or potential toxic metals are significant environmental pollutants, and their toxicity is a problem of increasing significance for ecological, evolutionary, nutritional, and environmental reasons. The term "heavy metals" refers to any metallic element that has a relatively high density and is toxic or poisonous even at low concentration [1]. Heavy metals, such as Pb(II), Hg(II), Cd(II), Co(II), Ni(II), and Cr(VI), are known to be prominent pollutants and even carcinogenic agents,

and may represent a serious threat to the living population because of their non-degradable, persistent, and accumulative nature [2–4]. The notorious itai-itai disease occurring in Japan during the 1960s and 1970s is one of the most famous accidents caused by chronic cadmium contaminated rice fields [5]. In recent decades, however, rare earth elements (REEs) were also widely exploited and used in industrial and high-tech fields as a result of their irreplaceable roles in designing magnetic, luminescent, catalytic, hydrogen storage, and superconductive materials [6–8]. More and more rare earth elements would inevitably enter into the environmental waters and work places, thus causing adverse health effects [9]. For instance, trivalent La(III) and Gd(III) ions can interfere with calcium channels in human and animal cells, also alter or even inhibit the action of various enzymes, and regulate synaptic transmission, as well as block some receptors (for example, glutamate receptors) when they are found in neurons [10,11]. Removal of the REEs entering the environment due to human activities has become a new concern [12–14]. Moreover, the small global reserve of REEs of no more than 99 million tons limits the wide use of REEs [15]. Hence, the recycling of REEs is also an urgent task [7].

The existing methods for the removal of heavy metals from the environment can be grouped into biotic and abiotic [16]. The biotic routes are based on the accumulation of the heavy metal by plants or microorganisms, while the abiotic ones mainly include physicochemical processes such as precipitation, co-precipitation, ion exchange, solvent extraction, electrolysis, reverse osmosis, and adsorption by a suitable sorbent. Because biotic accumulation by the present generation of plants and microorganisms is time consuming, fast removal of heavy metals from the environment and decontamination of drinking water still require abiotic or physicochemical methodologies [2,17]. Among the abiotic techniques, the adsorption process is cost effective, flexible, and easy to design and operate [4]. Clay minerals such as montmorillonite, kaolinite, vermiculite, sepiolite, etc., as dominant adsorptive materials, are widely used to capture metal ions from solutions, due to their high specific surface areas associated with their small particle size, low cost, and ubiquitous occurrence in most soil and sediment environments [4,16,18–25], and their adsorption for heavy metal ions proceeds mainly via ion exchange reactions and the formation of inner-sphere complexes through ≡Si–O– and ≡Al–O– groups at the clay particle edges [4,26]. However, the inherent limitations of clays as adsorbents of heavy metals are their low loading capacity, relatively small metal ion binding constants, and low selectivity to the type of metal [27].

To circumvent the inherent limitations, the modification of clay minerals with reagents containing metal chelating functional groups has become a prevalent and versatile means to enhance both their binding capacity and selectivity to heavy metals or organic pollutants [21,28]. After such modification, the adsorption of organic contaminants by clays is remarkably improved. However, their adsorption ability to heavy metals still remains relatively inefficient or limited. For example, Mercier and Pinnavaia [29] reported that when thiol groups were grafted to the interlamellar surface of magadiite and kenyaite, negligible heavy metal ion binding was observed. Celis et al. [16] found that 3-mercaptopropylsilyl-sepiolite and 2-mercaptoethylammonium-montmorillonite display higher adsorption capacity for Hg^{2+}, but significantly low adsorption capacity for Pb^{2+} and Zn^{2+} relative to their pure counterparts. Especially, the adsorption of montmorillonite functionalized by quaternary ammonium cations (QACs) toward heavy metals dramatically decreases compared with the raw montmorillonite, since the interlayer QACs are not readily exchangeable or the hydrophobic interlayer environment restrains the adsorption affinity for the hydrated metal cations [30,31]. Moreover, the modification processes are relatively complex, and organic solvents are usually needed [21,27,28,32]. Therefore, seeking facile clay modification methods to enhance the removal capacities for heavy metals is still a challenge.

Herein, a facile and environmentally friendly method was developed for modifying clay mineral sepiolite sequentially with acid and alkali to form a novel SiO_2–$Mg(OH)_2$ nanocomposite. Sepiolite was selected because it is fibrous hydrated magnesium silicate with the ideal chemical formula $Mg_4Si_6O_{15}(OH)_2{\cdot}6H_2O$ and is characterized by a high porosity and specific surface area [33]. Furthermore, mineral sepiolite has an alternation of blocks along its crystallographic [010] direction

and tunnels that grow up along its crystallographic [100] direction. Each structural block is built by two tetrahedral silica sheets with a central octahedral magnesia sheet [34,35]. The acid treatment investigations for sepiolite showed that variable amounts of structural Mg^{2+} ions can be removed, depending on the intensity of the acid treatment, while the tetrahedral silica sheets can form a free insoluble amorphous silica gel [36–39]. Therefore, it can be excepted that the in situ alkalization of the acid-treated sepiolite may produce the $Mg(OH)_2$-loaded amorphous silica composite. Moreover, nanostructured $Mg(OH)_2$ has also been proven to be an ideal water treatment agent to remove dyes and soluble heavy metals [7,40,41]. Therefore, the composite may possess improved removal performance to heavy metals and can be potentially applied in water treatment.

2. Materials and Methods

2.1. Materials and Chemicals

All chemical reagents were of analytical grade and used as received without any further purification. Hydrochloric acid (HCl), sodium hydroxide (NaOH), gadolinium oxide (Gd_2O_3), lead nitrate ($Pb(NO_3)_2$), and cadmium nitrate ($Cd(NO_3)_2$) were purchased from Sinopharm Chemical Reagent Co., Ltd. Raw sepiolite (Mg: ~13 wt %) was purchased from Sigma-Aldrich Chemical Reagent Co., Ltd. Deionized water was used in all the experiments.

2.2. Preparation of the SiO_2–$Mg(OH)_2$ Nanocomposite

Typical preparation processes of the SiO_2–$Mg(OH)_2$ nanocomposite were as follows: 5.0 g of sepiolite was first added into 100 mL of 5% (*v*/*v*) HCl solution (ca. 0.6 mol/L, pH = 0.22) at 60 °C for acid activation at a stirring speed of 300 r/min for 12 h, then 1.0 mol/L of NaOH solution was added dropwise to the solution under magnetic stirring until the pH of the solution reached 10.5. After 2 h of stirring, the suspension was centrifuged at 10,000 rpm for 10 min, and followed by washing with deionized water and absolute ethanol several times. Finally the precipitate was collected and dried at 50 °C under vacuum.

2.3. Characterizations

Several analytical techniques were used to characterize raw sepiolite and the treated products. X-ray diffraction (XRD) patterns were collected using a Japan Map XHF X-ray diffractometer equipped with graphite-monochromatized Cu Kα irradiation (λ = 0.154056 nm). FESEM images (FESEM) were obtained on a field-emission scanning electron microscopy JEOL JSM-2010. The size and structure of the samples were determined by a JEM-2010 transmission electron microscope (TEM) operating at 200 kV. Energy dispersive X-ray spectroscopy (EDX) analyses were obtained with an EDAX detector installed on the same TEM. N_2 adsorption–desorption isotherms were performed with a Micromeritics Coulter (USA) instrument utilizing Barrett–Emmett–Teller (BET) for specific surface area calculation.

2.4. Heavy Metal Removal

The removal abilities of the SiO_2–$Mg(OH)_2$ nanocomposite for rare earth element Gd(III) and traditional heavy metals Pb(II) and Cd(II) were studied by batch experiments. Stock solution with 10 mmol/L Gd(III) was prepared by dissolving gadolinium oxide (Gd_2O_3) in diluted hydrochloric acid. The Pb(II) or Cd(II) stock solution with a concentration of 10 mmol/L was obtained by dissolving $Pb(NO_3)_2$ or $Cd(NO_3)_2$ in deionized water. A series of solutions used during the removal experiments were prepared by diluting the stocks to the desired concentrations. Their actual concentrations were also measured using inductively coupled plasma atomic emission spectroscopy (ICP-AES, optima 7300 DV). Batch removal experiments for Gd(III), including the effects of pH and contact time were conducted in a 100 mL beaker equipped with a magnetic stirrer at a speed of 300 r/min. All of the beakers were covered with Parafilm. In a typical run, 50 mg of sorbent was mixed with 50 mL of solution containing Gd(III) at room temperature (293 K). The pH of the solution was adjusted with HCl

and/or NaOH solution before the sorbent addition, and measured using a pH meter (inoLab WTW series pH 740). The removal ability of the nanocomposite for Pb(II) and Cd(II) was investigated by the same procedure used for Gd(III) removal. The supernatant of the suspension was collected by centrifugation at 10,000 rpm for 10 min, and then filtered using a 0.22 μm pore size membrane filter. The concentration of Gd(II), Pb(II), or Cd(II) in the filtrate was determined by ICP-AES. The experiments were conducted in triplicate, and averaged values were reported. The content of heavy metal Gd(II), Pb(II), or Cd(II) removed at time t, q_t (mg/g), uptake percentage, U%, and the content of the heavy metal removed at equilibrium, q_e (mg/g), were calculated according to the following equations, respectively:

$$q_t = \frac{(C_o - C_t) \times V}{W}, \tag{1}$$

$$\mathrm{U\%} = \frac{(C_o - C_t) \times 100\%}{Co}, \tag{2}$$

$$q_e = \frac{(C_o - C_e) \times V}{W}, \tag{3}$$

where C_o (mg/L), C_t (mg/L), and C_e represent the liquid phase concentration of the heavy metal initially, at any time t, and at equilibrium, respectively. V is the volume of the solution (mL) and W is the mass of the sorbents added (mg).

3. Results and Discussion

3.1. Characterization of the SiO_2–$Mg(OH)_2$ Nanocomposite

The morphology and textures of raw sepiolite, acid-activated sepiolite, and sepiolite treated by sequential acid–base were first observed by FESEM and TEM techniques. The raw sepiolite had a nanofiber-like structure with a length of several micrometers and a width of ca. 30–40 nm (e.g., FESEM image in Figure S1a, TEM images in Figure 1a,b). The EDX spectrum showed that the rod-like sepiolite contains elements O, Si, and Mg, as well as C and Cu, here the elements C and Cu come from the carbon-coated Cu grid (inset in Figure 1b). After the acid activation of sepiolite in 5% (*v*/*v*) HCl solution at 60 °C for 12 h, a white colloid-like precipitate was obtained. Corresponding FESEM analyses show that the acid-activated sepiolite still exhibited the rod-like nanostructures (e.g., Figure S1b), but significant aggregation occurred compared to the raw sepiolite (e.g., Figure S1a). The TEM analyses further revealed that the morphological texture was still inherited from the raw sepiolite (e.g., Figure 1c). However, the magnified TEM image in Figure 1d unambiguously exhibits the distinct contrasts between the black lateral part and light middle part of the nanorods, unveiling that the space in the nanorods was significantly increased. Furthermore, the EDX result shows that no Mg^{2+} existed in the acid-activated sepiolite (Figure 1d inset), further confirming that the complete leaching of Mg^{2+} in octahedral sheets of sepiolite yielded the silica nanotubes (Figure 1d). For the products after the sequential acid–base treatment, one can find from the FESEM image (e.g., Figure S1c) that the surface of the product became rough with respect to raw sepiolite (Figure S1a) and acid-activated sepiolite (Figure S1b). The TEM results (Figure 1e,f) show that many neo-formed nanoneedles or nanosheets were anchored onto the silica nanotubes, distinct from the structures obtained after only the acid treatment (Figure 1c,d). The further-magnified TEM image (Figure 1f) reveals that the nanotubes were covered with many wrinkle nanosheets, and their width significantly increased. The EDX results (e.g., inset in Figure 1f) show that besides element O and Si, extra element Mg can be detected, suggesting that the neo-formed nanosheets were an Mg-bearing material.

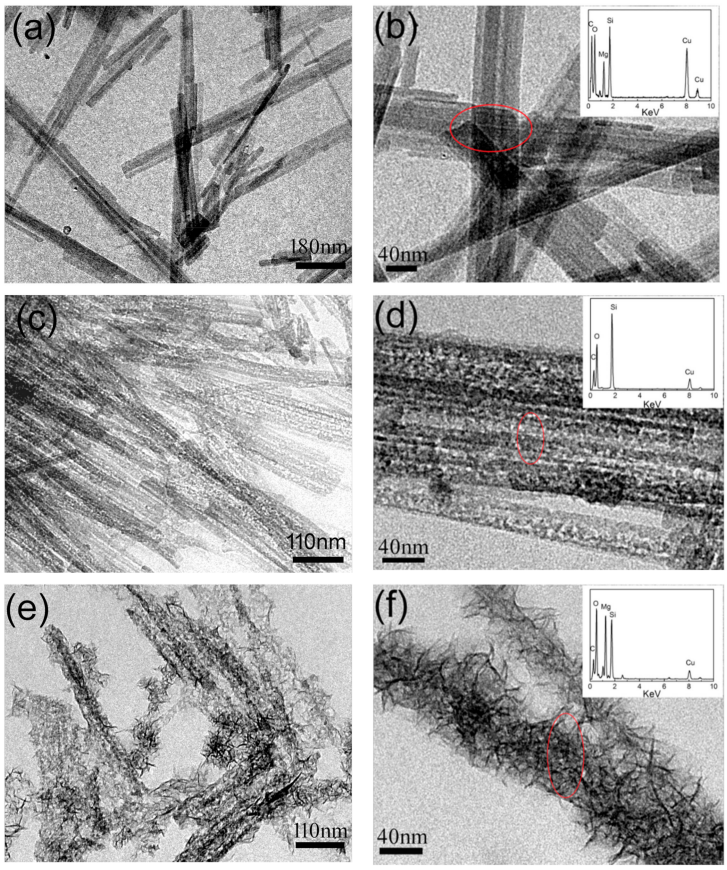

Figure 1. Typical TEM images of raw sepiolite (**a**,**b**), acid-activated sepiolite (**c**,**d**), and sepiolite modified by sequential acid–base treatment (**e**,**f**). Insets in panels b, d, and f are the corresponding energy dispersive X-ray spectroscopy (EDX) spectra. The red ellipses in Figure 1b,d,f indicate the areas of EDX analysis.

Figure 2 presents typical XRD patterns of raw sepiolite, acid-activated sepiolite, and sepiolite treated by sequential acid–base. The raw sepiolite exhibited the typical powder XRD pattern of pure sepiolite (JCPDF: 13-0595) (Figure 2a). For the acid-activated sepiolite, the characteristic peaks belonging to sepiolite disappeared, and a broad hump peak could be observed (Figure 2b), indicating that an amorphous phase formed. Combining with the EDX results (e.g., inset in Figure 1d), it can be concluded that the aggressive acid treatment led to the formation of amorphous silica nanotubes. However, after the sequential treatment of sepiolite with HCl and NaOH solutions, two broadened diffraction peaks in the XRD pattern could be identified, and these peaks can be indexed to the characteristic (001) and (100) diffractions of brucite ($Mg(OH)_2$, JCPDF: 07-0239) (Figure 2c), confirming that the leached Mg^{2+} from sepiolite can be precipitated as brucite after adding NaOH solution. The broadened diffraction peaks also support that the precipitated $Mg(OH)_2$ has a nanostructure (Figure 1e,f). Furthermore, the content of the $Mg(OH)_2$ in the SiO_2–$Mg(OH)_2$ nanocomposite was determined by ICP-AES after the sample was dissolved by HNO_3 solution, the result shows that up to 23.09 wt % of $Mg(OH)_2$ was loaded on the surface of the rod-like silica, indicating that the leached Mg^{2+} was precipitated as $Mg(OH)_2$ nanosheets anchored to the SiO_2 nanotubes, finally forming a hierarchical $Mg(OH)_2$–SiO_2 nanocomposite.

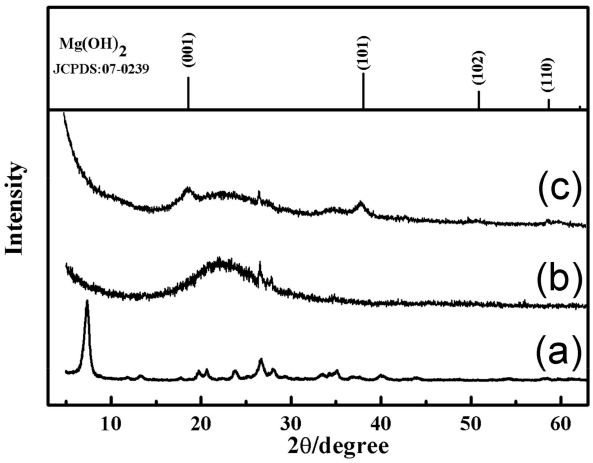

Figure 2. Representative XRD patterns of raw sepiolite (**a**), acid-activated sepiolite (**b**), and sepiolite modified by sequential acid–base treatment (**c**).

Figure 3 further shows the representative FTIR spectra of raw sepiolite, the amorphous SiO_2 nanotubes, and the $Mg(OH)_2$–SiO_2 nanocomposite. As shown in Figure 3a, the vibrational bands located in the 4000–400 cm^{-1} range can all be assigned to the characteristic vibrations of clay mineral sepiolite, i.e., the vibrations of the Mg–OH group (3690 cm^{-1}), coordinated water (3568 cm^{-1}), zeolitic water (3422 cm^{-1}, 1650 cm^{-1}); and the bonds of Si–O–Si (1016 and 460 cm^{-1}), Si–O (1215, 1076 cm^{-1} (shoulder), and 973 cm^{-1}), Si–O–Mg (437 cm^{-1}), and Mg–O (690 and 637 cm^{-1}) [37,38]. After the acid treatment, the intensity of bands in the 4000–3000 cm^{-1} range and at 1650 cm^{-1} were decreased. The wide band centered at 1016 cm^{-1} (actually consisting of four different bands at 1215, 1076, 1016, and 973 cm^{-1}) changed its form, and shifted to higher wave numbers, from 1016 to 1085 cm^{-1}, indicating the textural changes in the solids (Figure 3b) [37]. The peaks at 1081, 800, and 460 cm^{-1} agreed with the Si–O–Si bond [42,43], confirming that the natural sepiolite transformed into silica after the acid activation, consistent with the EDX results (e.g., inset in Figure 1d). As for the $Mg(OH)_2$–SiO_2 composite, one can find from Figure 3c that the peak locations have no obvious changes relative to the silica (Figure 3b), except for the increase in the intensities of the bands in the 4000–3000 cm^{-1} and 700–600 cm^{-1} ranges, which usually are indicative for Mg–OH bond vibrations [37], confirming the formation of $Mg(OH)_2$ precipitate after the base treatment.

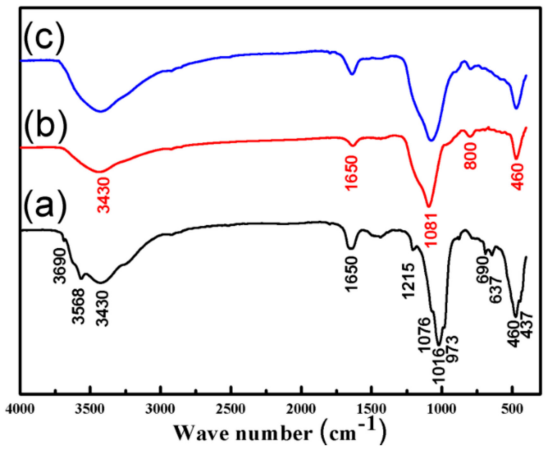

Figure 3. FTIR spectra of raw sepiolite (**a**), amorphous SiO_2 nanotubes (**b**), and $Mg(OH)_2$–SiO_2 composite (**c**).

Representative N_2 adsorption–desorption isotherms are shown in Figure 4 for the raw sepiolite, amorphous SiO_2, and SiO_2–$Mg(OH)_2$ nanocomposite, respectively. It can be seen that all the specimens

showed a type IV N_2 adsorption isotherm with an evident hysteresis loop, suggesting the presence of mesopores in the materials [44]. After the acid activation of raw sepiolite, the BET surface area and total pore volume of the formed amorphous SiO_2 increased from 256.5 m^2/g and 0.47 cm^3/g to 488.5 m^2/g and 0.87 cm^3/g, this could be attributed to the acid leaching of Mg^{2+} from the sepiolite and the formation of silica with central channels (Figure 1e,f). For the hierarchical SiO_2–$Mg(OH)_2$ nanocomposite, the surface area and total pore volume were 377.3 m^2/g and 0.96 cm^3/g, respectively. The relative lower surface area of the nanocomposite with respect to the amorphous silica nanotubes should arise from the formation of nanosized $Mg(OH)_2$ on the silica nanotube surfaces (Figure 1e,f).

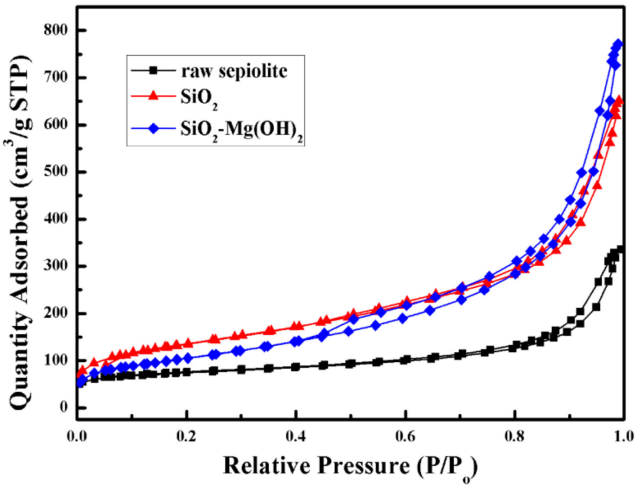

Figure 4. N_2 adsorption/desorption isotherms of raw sepiolite (black), amorphous SiO_2 nanotubes (red), and $Mg(OH)_2$–SiO_2 composite (blue).

3.2. Removal of Gd(III) by SiO_2–$Mg(OH)_2$ Nanocomposite

It is well known that $Mg(OH)_2$ would dissolve under a low-pH circumstance [45], and the precipitation of heavy metals hydroxides can also occur at higher pH values. Therefore, the parameter pH is usually believed to be one of the most important factors affecting the adsorption process. Here, in order to avoid the dissolution of $Mg(OH)_2$ and the precipitation of Gd(III) hydroxide, $Ksp_{Gd(OH)3}$ is 8.2×10^{-23} at 25 °C [46], a pH range from 3.0 to 7.5 was selected, and the concentration of Gd(III) solution 0.1 mmol/L (ca. 15.2 mg/L) was used. The desired initial pH values were adjusted before the addition of the sorbent into the Gd(III) solution. One can find from Figure 5a that the Gd(III) was almost completely removed by the nanocomposite over the wide pH range. For the raw sepiolite, however, the removal percentages of Gd(III) were lower than the nanocomposite, especially at low pHs, indicating that the nanocomposite has excellent removal efficiency over the raw sepiolite. Usually, the surface charge of the adsorbent is believed to play a crucial role in adsorption [14,35]. As is known, the point of zero charge (PZC) is an important property of the adsorbent as the surfaces acquire negative charge at pH values higher than the pH at PZC (pHpzc). The pHpzc for sepiolite is about 7.4 [37]. Therefore, the low Gd(III) uptakes of raw sepiolite at low pH values were most probably due to the protonation of the active sites in sepiolite, which inhibited their binding toward Gd(III) [35]. As pH increases, however, the surface positive charge of adsorbent sepiolite decreases, and thus the uptake of Gd(III) increases. As for the SiO_2–$Mg(OH)_2$ nanocomposite, the pHpzc value was close to 1.5 (Figure S2), measured by a Zeta potential analyzer, and the nanocomposite had higher surface area than the raw sepiolite. These dominate the almost complete removal of Gd(III) by the nanocomposite over the used pH range. Figure 5b further shows their pH evolution relationships before and after adsorption. It can be found that the final pH values rose significantly after removal treatment by the SiO_2–$Mg(OH)_2$ nanocomposite relative to the raw sepiolite. This was possible because the $Mg(OH)_2$ in the nanocomposite has a basic nature, thereby producing a level-off effect on the pH of the Gd(III) removal system. As a result, a high final pH 9.7 was always achieved over the initial pH range

3–7.5; as was the case in the Ag_2O–$Mg(OH)_2$ nanocomposite for I^- removal [41]. According to the pH-dependent experiments, a neutral pH 7.0 was selected in the following removal experiments.

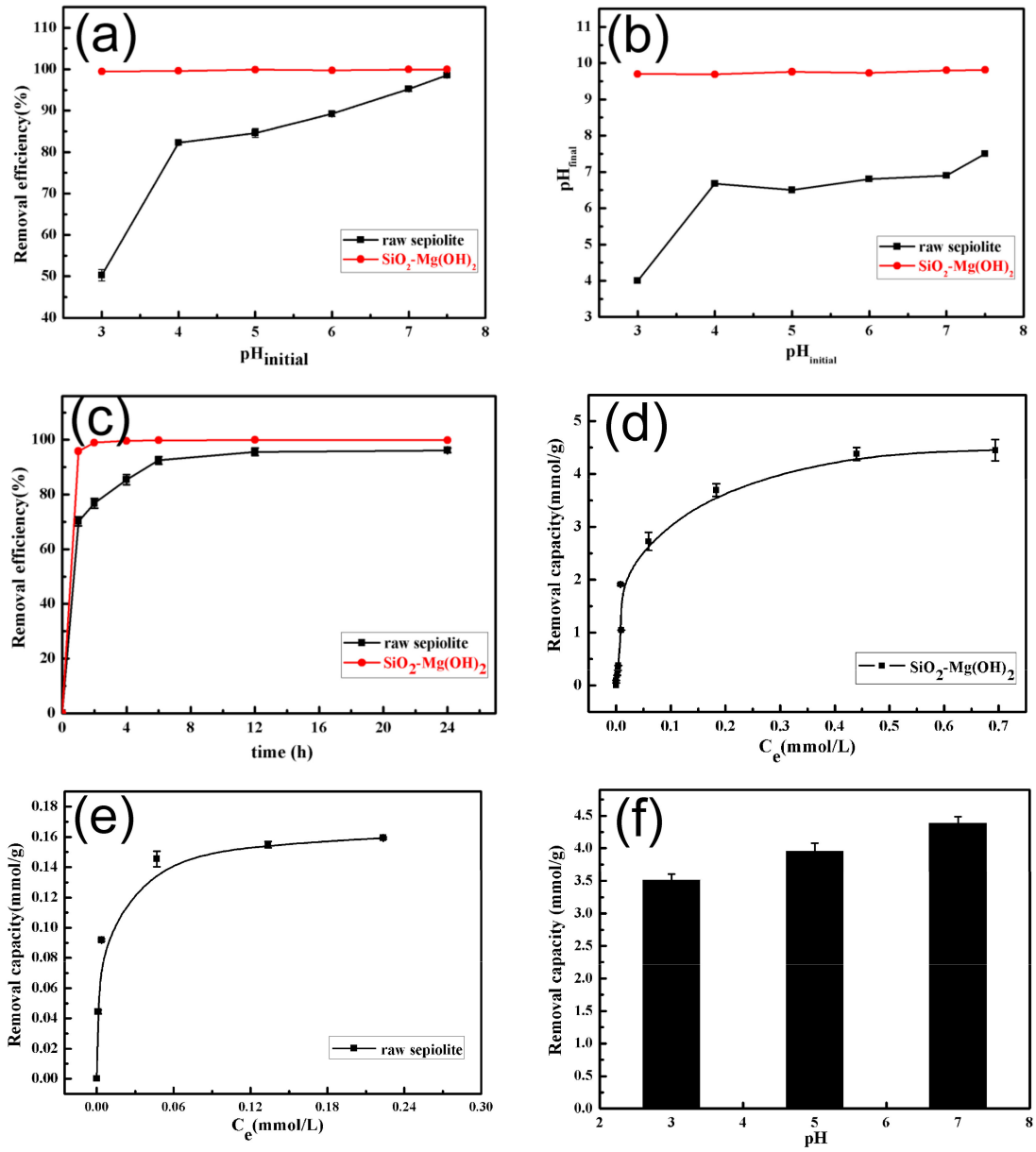

Figure 5. Effect of pH on the removal efficiency of Gd(III) by raw sepiolite and the SiO_2–$Mg(OH)_2$ nanocomposite (**a**); relationship between the initial and final pH of the adsorption system (**b**); effect of contact time on the Gd(III) removal by raw sepiolite and the nanocomposite (**c**); removal capacity of the nanocomposite (**d**) and raw sepiolite (**e**) for Gd(III); removal capacity of the nanocomposite for Gd(III) at different pHs (**f**).

Figure 5c presents the performance of Gd(III) removal by the SiO_2–$Mg(OH)_2$ nanocomposite and raw sepiolite versus contact time at the initial Gd(III) concentration of 0.1 mmol/L. It is not difficult to find that the Gd(III) removal rapidly increased in the presence of the nanocomposite, and almost all Gd(III) was removed in the first 120 min. In contrast, only 78% of Gd(III) was removed for the raw sepiolite, and the final removal efficiency for Gd(III) was also lower than that by the nanocomposite. In most wastewater, the REE concentrations are as low as one to hundreds of mg/L, despite the high total annual wastewater generation of more than 7.2 million tons [7]. Traditional adsorbents, e.g., zeolite, clay, and active carbon, donate high adsorption capacities only at high metal ion concentrations,

but they are usually not suitable for dilute metal ion solutions because of their weak extraction force [47]. In this regard, the SiO_2–$Mg(OH)_2$ nanocomposite derived from sepiolite has great potential for the removal and enrichment treatment of low-concentration REEs and even other heavy metals. Moreover, the removal capacities of the nanocomposite and raw sepiolite for Gd(III) were also tested at neutral pH and room temperature. As shown in Figure 5d, the nanocomposite had an amazing removal capacity for Gd(III), ca. 4.45 mmol/g (ca. 698.65 mg/g), but only 0.159 mmol/g (ca. 24.96 mg/g) for the raw sepiolite (Figure 5e), indicating that the Gd (III) removal ability of the sepiolite treated by sequential acid—base was greatly enhanced. Especially at pH 3.0 and 5.0, the removal capacity toward Gd(III) of the nanocomposite still reached 3.52 and 4.1 mmol/g (e.g., Figure 5f), indicating its superb removal ability for Gd(III) over the wide pH range. As the REEs and some trivalent actinides have similar chemical behavior, this removal reagent should also be useful for other lanthanide and actinide elements.

3.3. Removal Abilities of SiO_2–$Mg(OH)_2$ Nanocomposite for Pb(II) and Cd(II)

Lazarević et al. [37] studied the adsorption of Pb(II) and Cd(II) on natural sepiolite and the influence of acid activation treatment on the adsorption capacity. Their results indicated that raw sepiolite is more effective for the adsorption of Pb(II) and Cd(II) than acid-activated sepiolite, i.e., the adsorption ability of natural sepiolite for Pb(II) and Cd(II) is 0.35 and 0.23 mmol/g, respectively; whereas the sepiolite activated by a 4 M of HCl solution for 10 h at room temperature only has 0.22 mmol/g for Pb(II), and 0.21 mmol/g for Cd(II). They proposed that the retention of Pb(II) and Cd(II) occurs dominantly by specific adsorption and exchange of Mg^{2+} ions from the sepiolite structure, and the lowered removal performance of the acid-activated sepiolite can be ascribed to the decrease in the number of Mg–OH groups as main centers for specific adsorption and the number of Mg^{2+} ions available for ion exchange with cations [37]. Herein, the removal ability of the SiO_2–$Mg(OH)_2$ nanocomposite for Pb(II) and Cd(II) was also tested by similar removal experiments at pH 5.6, as described by Lazarević et al. [37]. As shown in Figure 6, the removal capacity of the SiO_2–$Mg(OH)_2$ nanocomposite for Pb(II) and Cd(II) was 6.84 and 4.88 mmol/g, respectively, which are much higher than the removal capacities of the natural and acid-activated sepiolite [37]. This is possible because the $Mg(OH)_2$ nanosheets anchored onto the nanocomposite increased the Mg^{2+} availability and exchangeability, leading to the high removal capacities. The current results also indicate that after the facile modification, the removal ability of sepiolite for other common heavy metals would be greatly enhanced.

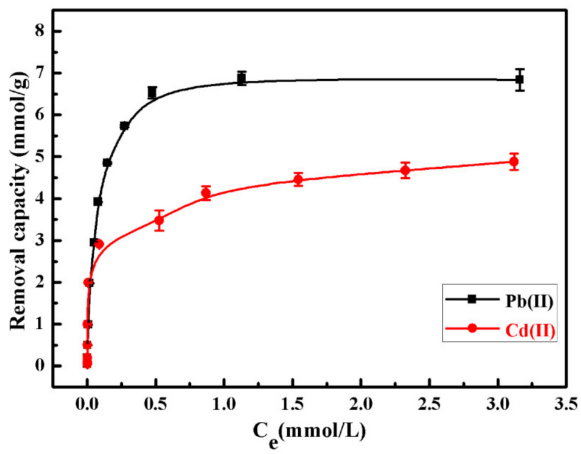

Figure 6. Removal capacities of the SiO_2–$Mg(OH)_2$ nanocomposite for Pb(II) and Cd(II) at pH 5.6.

3.4. Removal Mechanism of SiO_2–$Mg(OH)_2$ Nanocomposite for Heavy Metals

In order to understand the removal mechanism of heavy metal cations (Me^{n+}) by the SiO_2–$Mg(OH)_2$ nanocomposite, numerous techniques including FESEM, TEM, EDX, XRD, and FTIR, were used to characterize the samples after the heavy metal immobilization. As shown in Figure 7a, the Gd(III)-loaded

nanocomposite still exhibited rod-like structures, and numerous small particles adhering on the nanocomposite surface could be found (as indicated by the red circle). The TEM image further revealed that the tube-like SiO_2 were covered with many isolated nanoparticles (Figure 7b), and the element Gd was also detected by the EDX analysis (e.g., inset in Figure 7b), indicating that the particles on the nanocomposite surfaces were Gd(III)-bearing precipitate. Further, the XRD analyses exhibited an obvious hump peak, which was similar to the pattern of acid-activated sepiolite (e.g., Figure 2b), and no diffraction peaks belonging to the known gadolinium compounds, especially gadolinium hydroxide were detected. However, the FTIR spectrum displayed two extra bands at 1520 and 1412 cm^{-1} (Figure 7d) in comparison with the FTIR spectrum of the SiO_2–$Mg(OH)_2$ nanocomposite (Figure 3c), which could be assigned to the bidentate asymmetric band of C–O–O and the bidentate symmetric band of C–O–O, respectively [48–50]. These results indicated that the Gd(III)-bearing compound formed in the removal processes may be Gd(III) carbonates. Therefore, the removal mechanism of Me^{n+} may be via sorption and the subsequent precipitation of Me-containing carbonates on the composite surface. To verify the deduction, the samples after the Pb(II) and Cd(II) removal by SiO_2–$Mg(OH)_2$ nanocomposite were also characterized by FESEM and XRD. Similarly, many small grains could be observed from the FESEM images after the Pb and Cd removal by the nanocomposite (Figure S3a,b), indicating the formation of Me-bearing compounds. The corresponding XRD results clearly revealed that all the peaks in XRD patterns could be indexed to hydrocerussite ($Pb_3(CO_3)_2(OH)_2$, JCPDS: 13-0131) (Figure 7e) and otavite ($CdCO_3$, JCPDS: 42-1342) (Figure 7f), respectively. The results confirmed the removal mechanism of SiO_2–$Mg(OH)_2$ nanocomposite to heavy metals via a heavy metal carbonatation on its surfaces. Therefore, the superb removal capacity of SiO_2–$Mg(OH)_2$ nanocomposite toward heavy metals could be attributed to the synergistic effect of nano-$Mg(OH)_2$ and amorphous SiO_2 nanotubes in SiO_2–$Mg(OH)_2$ composite. The SiO_2 nanotubes, obtained by complete acid-activated of sepiolite, possessed high surface area and acted as a support substrate. The $Mg(OH)_2$ nanosheets, formed by the reprecipitation of the leached Mg ions from sepiolite, acted as a reactive reagent in heavy metal removal. During the removal processes, the heavy metals were first adsorbed onto the SiO_2–$Mg(OH)_2$ composite by Mg^{2+} exchange with Me^{n+}, and then the nano-$Mg(OH)_2$ with basic nature promoted the intake of CO_2, leading to Me-containing carbonates on the nanocomposite.

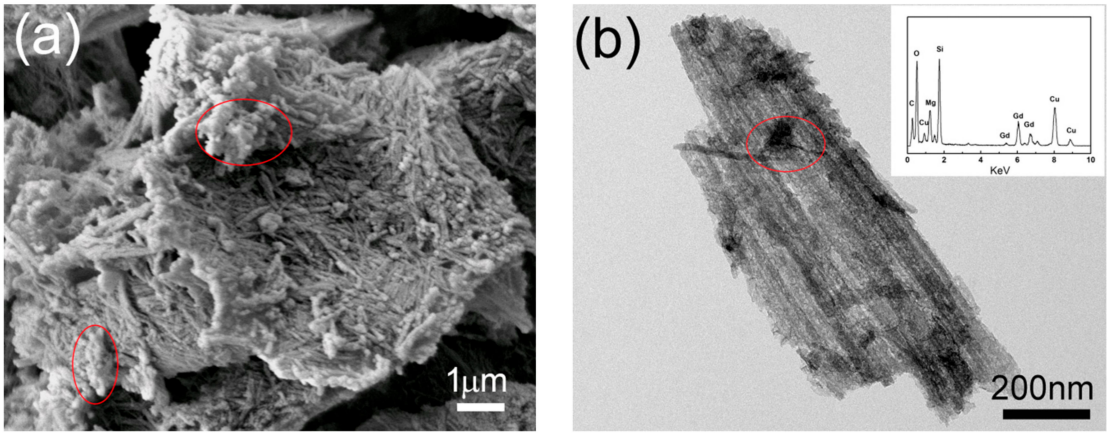

Figure 7. *Cont.*

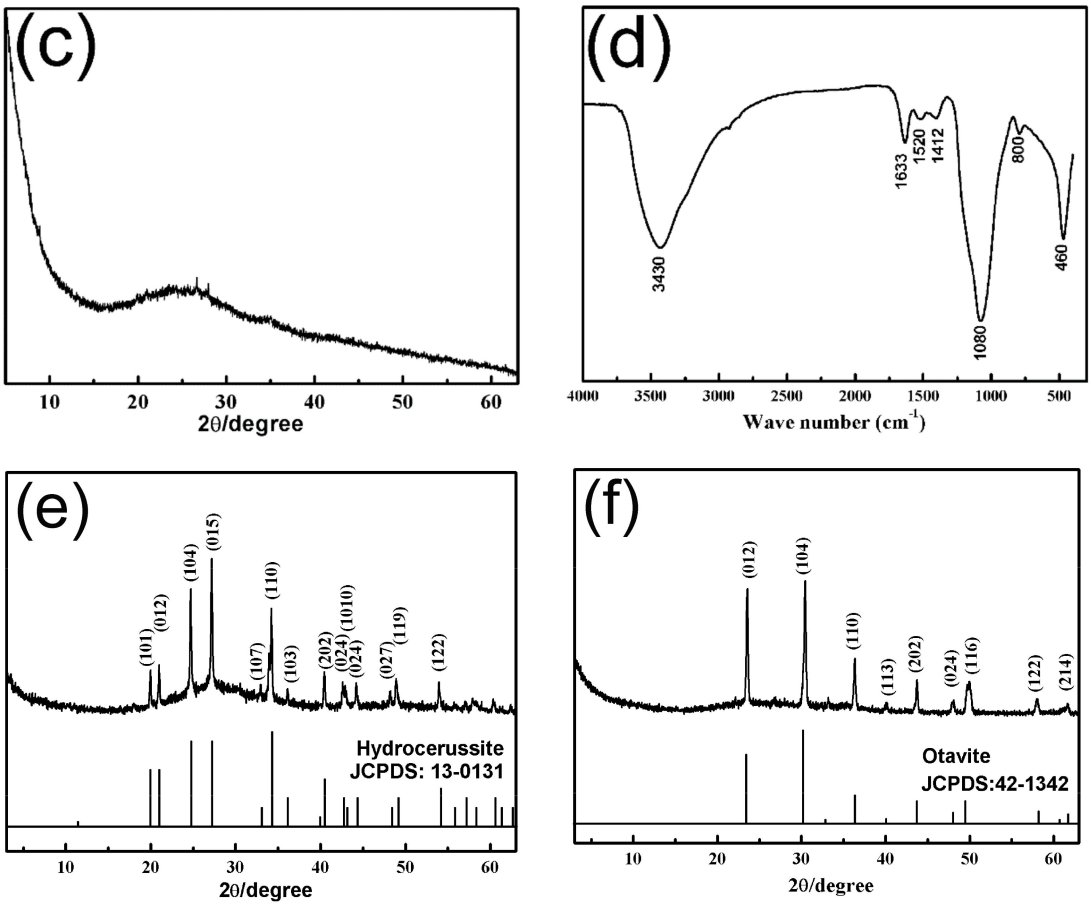

Figure 7. FESEM (**a**) and TEM (**b**) images, XRD pattern (**c**), and FTIR spectrum (**d**) of Gd(III)-loaded SiO_2–$Mg(OH)_2$ nanocomposite; XRD patterns of Pb(II)-loaded SiO_2–$Mg(OH)_2$ nanocomposites (**e**); and Cd(II)-loaded SiO_2–$Mg(OH)_2$ nanocomposites (**f**). The red ellipses in Figure 7a,b highlight the small particles adhering to the nanocomposite surface.

4. Conclusions

In summary, the hierarchical SiO_2–$Mg(OH)_2$ nanocomposite was successfully obtained by sequential acid–base treatment of natural sepiolite. First, the acid treatment led to the rod-like amorphous silica with central channels due to the Mg^{2+} leaching out of sepiolite. After adding the base agent, the leached Mg^{2+} further precipitated into sheet-like $Mg(OH)_2$ on the silica nanotube surfaces, finally producing the hierarchical nanocomposite. The SiO_2–$Mg(OH)_2$ nanocomposite with high surface area and pore volume exhibited an amazing removal capacity for Gd(III) (ca. 4.45 mmol/g), which was about 28 times of that of raw sepiolite (0.159 mmol/g). Moreover, this nanocomposite also showed exceptional removal capacity for common heavy metals (6.84 mmol/g for Pb^{2+}, 4.88 mmol/g for Cd^{2+}). The superb removal capacity of the SiO_2–$Mg(OH)_2$ nanocomposite toward heavy metals can be attributed to the synergistic effects of the two nanostructure components in the nanocomposite, i.e., the removal of the heavy metals proceeds via the initial sorption and subsequent carbonatation of heavy metal ions on the nanocomposite surface. The removal capacity of sepiolite to heavy metals was greatly enhanced after the sequential acid–base modification. As the modification method is facile and suitable for large scale preparation, the SiO_2–$Mg(OH)_2$ nanocomposite derived from sepiolite has real potential for applications in water treatment.

Supplementary Materials: The following are available online at http://www.mdpi.com/2075-163X/9/5/298/s1, Figure S1: Typical SEM images of raw sepiolite, acid-activated sepiolite, and sepiolite modified by sequential acid–base treatment; Figure S2: Zeta potential-pH profile for the SiO_2–$Mg(OH)_2$ nanocomposite

in deionized water; Figure S3: SEM images of Pb(II)-loaded SiO_2–$Mg(OH)_2$ nanocomposite and Cd(II)-loaded SiO_2–$Mg(OH)_2$ nanocomposite.

Author Contributions: Conceptualization, Q.-Z.Y. and S.-H.Y.; methodology, Q.-Z.Y.; validation, S.-H.Y. and G.-T.Z.; formal analysis, T.-L.Z.; F.-J.Q., H.L., and S.-Q.F.; investigation, Q.-Z.Y and S.H.Y.; data curation, Q.-Z.Y., S.-H.Y., and G.-T.Z.; writing—original draft preparation, Q.-Z.Y.; writing—review and editing, S.-H.Y. and G.-T.Z.; supervision, G.-T.Z.; funding acquisition, Q.-Z.Y., H.L., S.-H.Y., and G.-T.Z.

Funding: This work was partially supported by the National Natural Science Foundation of China (Nos. 41672034, 41702038, and 41772030), and the Specialized Research Fund for the Doctoral Program of Higher Education (No. 20133402130007).

Conflicts of Interest: The authors declare no conflict of interest.

References

1. Nagajyoti, P.C.; Lee, K.D.; Sreekanth, T.V.M. Heavy metals, occurrence and toxicity for plants: A review. *Environ. Chem. Lett.* **2010**, *8*, 199–216. [CrossRef]
2. Kocaoba, S. Adsorption of Cd(II), Cr(III) and Mn(II) on natural sepiolite. *Desalination* **2009**, *244*, 24–30. [CrossRef]
3. Fabbricino, M.; Ferraro, A.; Luongo, V.; Pontoni, L.; Race, M. Soil washing optimization, recycling of the solution, and ecotoxicity assessment for the remediation of Pb-Contaminated sites using EDDS. *Sustainability* **2018**, *10*, 636. [CrossRef]
4. Uddin, M.K. A review on the adsorption of heavy metals by clay minerals, with special focus on the past decade. *Chem. Eng. J.* **2017**, *308*, 438–462. [CrossRef]
5. Kaji, M. Role of experts and public participation in pollution control: the case of Itai-itai disease in Japan. *Ethics Sci. Environ. Polit.* **2012**, *12*, 99–111. [CrossRef]
6. Ali, O.I.M.; Osman, H.H.; Sayed, S.A.; Shalabi, M.E.H. The removal of some rare earth elements from their aqueous solutions on by-pass cement dust (BCD). *J. Hazard. Mater.* **2011**, *195*, 62–67. [CrossRef] [PubMed]
7. Li, C.; Zhang, Z.; Huang, F.; Wu, Z.; Hong, Y.; Lin, Z. Recycling rare earth elements from industrial wastewater with flowerlike nano-$Mg(OH)_2$. *ACS Appl. Mater. Interfaces* **2013**, *5*, 9719–9725. [CrossRef] [PubMed]
8. Charalampides, G.; Vatalis, K.I.; Apostoplos, B.; Ploutarch-Nikolas, B. Rare earth elements: Industrial applications and economic dependency of Europe. *Procedia Econ. Finance* **2015**, *24*, 126–135. [CrossRef]
9. Aghayan, H.; Mahjoub, A.R.; Khanchi, A.R. Samarium and dysprosium removal using 11-molybdo-vanadophosphoric acid supported on Zr modified mesoporous silica SBA-15. *Chem. Eng. J.* **2013**, *225*, 509–519. [CrossRef]
10. Pałasz, A.; Czekaj, P. Toxicological and cytophysiological aspects of lanthanides Action. *Acta Biochim. Pol.* **2000**, *47*, 1107–1114. [PubMed]
11. Chen, Z.Y.; Zhu, X.Z. Accumulation of rare earth elements in bone and its toxicity and potential hazard to health. *J. Ecol. Rural Environ.* **2008**, *24*, 88–91.
12. Tan, X.; Fan, Q.; Wang, X.; Grambow, B. Eu(III) sorption to TiO_2 (anatase and rutile): batch, XPS, and EXAFS studies. *Environ. Sci. Technol.* **2009**, *43*, 3115–3121. [CrossRef] [PubMed]
13. Yesiller, S.U.; Eroğlu, A.E.; Shahwan, T. Removal of aqueous rare earth elements (REEs) using nano-iron based materials. *J. Ind. Eng. Chem.* **2013**, *19*, 898–907. [CrossRef]
14. Yu, S.H.; Yao, Q.Z.; Zhou, G.T.; Fu, S.Q. Preparation of hollow core/shell microspheres of hematite and its adsorption ability for samarium. *ACS Appl. Mater. Interfaces* **2014**, *6*, 10556–10565. [CrossRef] [PubMed]
15. Chen, Z.J. Global rare earth resources and scenarios of future rare earth industry. *J. Rare Earth* **2011**, *2*, 1–6. [CrossRef]
16. Celis, R.; Hermosin, M.C.; Cornejo, J. Heavy metal adsorption by functionalized clays. *Environ. Sci. Technol.* **2000**, *34*, 4593–4599. [CrossRef]
17. Lothenbach, B.; Furrer, G.; Schulin, R. Immobilization of heavy metals by polynuclear aluminium and montmorillonite compounds. *Environ. Sci. Technol.* **1997**, *31*, 1452–1462. [CrossRef]
18. Bailey, S.E.; Olin, T.J.; Bricka, R.M.; Adrian, D.D. A review of potentially low-cost sorbents for heavy metals. *Water Res.* **1999**, *33*, 2469–2479. [CrossRef]
19. Yuan, P.; Li, D.; Fan, M.; Yang, D.; Zhu, R.; Ge, F.; Zhu, J.; He, H. Removal of hexavalent chromium [Cr(VI)] from aqueous solutions by the diatomite-supported/unsupported magnetite nanoparticles. *J. Hazard. Mater.* **2010**, *173*, 614–621. [CrossRef]

20. Arancibia-Miranda, N.; Baltazar, S.E.; García, A.; Muñoz-Lira, D.; Sepúlveda, P.; Rubio, M.A.; Altbir, D. Nanoscale zero valent supported by Zeolite and Montmorillonite: Template effect of the removal of lead ion from an aqueous solution. *J. Hazard. Mater.* **2016**, *301*, 371–380. [CrossRef] [PubMed]
21. Zhu, L.; Wang, L.; Xu, Y. Chitosan and surfactant co-modified montmorillonite: A multifunctional adsorbent for contaminant removal. *Appl. Clay Sci.* **2017**, *146*, 35–42. [CrossRef]
22. Doğan, M.; Turhan, Y.; Alkan, M.; Namli, H.; Turan, P.; Demirbaş, Ö. Functionalized sepiolite for heavy metal ions adsorption. *Desalination* **2008**, *230*, 248–268. [CrossRef]
23. García, N.; Guzmán, J.; Benito, E.; Esteban-Cubillo, A.; Aguilar, E.; Santarén, J.; Tiemblo, P. Surface modification of sepiolite in aqueous gels by using methoxysilanes and its impact on the nanofiber dispersion ability. *Langmuir* **2011**, *27*, 3952–3959. [CrossRef] [PubMed]
24. Hu, B.; Hu, Q.; Chen, C.; Sun, Y.; Xu, D.; Sheng, G. New insights into Th(IV) speciation on sepiolite: Evidence for EXAFS and modeling investigation. *Chem. Eng. J.* **2017**, *322*, 66–72. [CrossRef]
25. Kara, M.; Yuzer, H.; Sabah, E.; Celik, M.S. Adsorption of cobalt from aqueous solutions onto sepiolite. *Water Res.* **2003**, *37*, 224–232. [CrossRef]
26. Sheng, G.; Xu, S.; Boyd, S.A. A dual function organoclay sorbent for lead and chlorobenzene. *Soil Sci. Soc. Am. J.* **1999**, *63*, 73–78. [CrossRef]
27. Mercier, L.; Detellier, C. Preparation, characterization, and applications as heavy metals sorbents of covalently grafted thiol functionalities on the interlamellar surface of montmorillonite. *Environ. Sci. Technol.* **1995**, *29*, 1318–1323. [CrossRef] [PubMed]
28. Yang, J.; Yu, K.; Liu, G. Chromium immobilization in soil using quaternary ammonium cations modified montmorillonite: Characterization and mechanism. *J. Hazard. Mater.* **2017**, *321*, 73–80. [CrossRef] [PubMed]
29. Mercier, L.; Pinnavaia, T.J. Heavy metal ion adsorbents formed by the grafting of a thiol functionality to mesoporous silica molecular sieves: Factors affecting Hg(II) uptake. *Environ. Sci. Technol.* **1998**, *32*, 2749–2754. [CrossRef]
30. Theng, B.K.G.; Churchman, G.J.; Gates, W.P.; Yuan, G.D. Organically Modified Clays for Pollutant Uptake and Environmental Protection. In *Soil Mineral Microbe-Organic Interactions*; Huang, Q., Huang, P., Violante, A., Eds.; Springer: Berlin/Heidelberg, Germany, 2008; pp. 145–174.
31. Ma, L.; Chen, Q.; Zhu, J.; Xi, Y.; He, H.; Zhu, R.; Tao, Q.; Ayoko, G.A. Adsorption of phenol and Cu(II) onto cationic and zwitterionic surfactant modified montmorillonite in single and binary systems. *Chem. Eng. J.* **2016**, *283*, 880–888. [CrossRef]
32. Liang, X.; Xu, Y.; Sun, G.; Wang, L.; Sun, Y.; Sun, Y.; Qin, X. Preparation and characterization of mercapto functionalized sepiolite and their application for sorption of lead and cadmium. *Chem. Eng. J.* **2011**, *174*, 436–444. [CrossRef]
33. Al-Ani, A.; Gertisser, R.; Zholobenko, V. Structural features and stability of Spanish sepiolite as a potential catalyst. *Appl. Clay Sci.* **2018**, *162*, 297–304. [CrossRef]
34. Wan, C.Y.; Chen, B.Q. Synthesis and characterization of biomimetic hydroxyapatite/sepiolite nanocomposites. *Nanoscale* **2011**, *3*, 693–700. [CrossRef] [PubMed]
35. Yu, S.H.; Li, H.; Yao, Q.Z.; Zhou, G.T.; Fu, S.Q. Microwave-assisted preparation of sepiolite-supported magnetite nanoparticles and their ability to remove low concentrations of Cr(VI). *RSC Adv.* **2015**, *5*, 84471–84482. [CrossRef]
36. Aznar, A.J.; Gutiérrez, E.; Díaz, P.; Alvarez, A.; Poncelet, G. Silica from sepiolite: Preparation, textural properties, and use as support to catalysts. *Microporous Mater.* **1996**, *6*, 105–114. [CrossRef]
37. Lazarević, S.; Janković-Častvan, I.; Jovanović, D.; Milonjić, S.; Janaćković, D.; Petrović, R. Adsorption of Pb^{2+}, Cd^{2+} and Sr^{2+} ions onto natural and acid-activated sepiolites. *Appl. Clay Sci.* **2007**, *37*, 47–57. [CrossRef]
38. Myriam, M.; Suaárez, M.; Martín-Pozas, J.M. Structural and textural modifications of palygorskite and sepiolite under acid treatment. *Clay Clay Miner.* **1998**, *46*, 225–231. [CrossRef]
39. Franco, F.; Pozo, M.; Cecilia, J.A.; Benítez-Guerrrero, M.; Pozo, E.; Martín-Rubí, J.A. Microwave assisted acid treatment of sepiolite: The role of composition and crystallinity. *Appl. Clay Sci.* **2014**, *102*, 15–27. [CrossRef]
40. Liu, W.; Huang, F.; Wang, Y.; Zou, T.; Zheng, J.; Lin, Z. Recycling $Mg(OH)_2$ nanoadsorbent during treating the low concentration of Cr^{VI}. *Environ. Sci. Technol.* **2011**, *45*, 1955–1961. [CrossRef]
41. Chen, Y.Y.; Yu, S.H.; Yao, Q.Z.; Fu, S.Q.; Zhou, G.T. One-step synthesis of $Ag_2O@Mg(OH)_2$ nanocomposite as an efficient scavenger for iodine and uranium. *J. Colloid. Interf. Sci.* **2018**, *510*, 280–291. [CrossRef] [PubMed]
42. Venkatathri, N.; Srivastava, R.; Yun, D.S.; Yoo, J.W. Synthesis of a novel class of mesoporous hollow silica from organic templates. *Micropor. Mesopor. Mat.* **2008**, *112*, 147–152. [CrossRef]

43. Shi, J.Y.; Yao, Q.Z.; Li, X.M.; Zhou, G.T.; Fu, S.Q. Formation of asymmetrical structured silica controlled by a phase separation process and implication for Biosilicification. *PLoS ONE* **2013**, *8*, e61164. [CrossRef] [PubMed]
44. Liu, H.C.; Chen, W.; Liu, C.; Liu, Y.; Dong, C.L. Magnetic mesoporous clay adsorbent: Preparation, characterization and adsorption capacity for atrazine. *Microporous Mesoporous Mater.* **2014**, *194*, 72–78. [CrossRef]
45. Pokrovsky, O.S.; Schott, J. Experimental study of brucite dissolution and precipitation in aqueous solutions: Surface speciation and chemical affinity control. *Geochim. Cosmochim. Acta* **2004**, *68*, 31–45. [CrossRef]
46. Moeller, T.; Fogel, N. Observations on the rare earths. LXI. precipitation of hydrous oxides or hydroxides from perchlorate solutions. *JACS* **1951**, *73*, 4481. [CrossRef]
47. Babel, S.; Kurniawan, T.A. Low-cost adsorbents for heavy metals uptake from contaminated water: A review. *J. Hazard. Mater.* **2003**, *97*, 219–243. [CrossRef]
48. Yanagihara, N.; Vemulapalli, K.; Fernando, Q.; Dyke, J.T. Synthesis of lanthanide carbonates. *J. Less Common Met.* **1991**, *167*, 223–232. [CrossRef]
49. Wu, Y.; Xu, X.; Tang, Q.; Li, Y. A new type of silica-coated $Gd_2(CO_3)_3$: Tb nanoparticle as a bifunctional agent for magnetic resonance imaging and fluorescent imaging. *Nanotechnology* **2012**, *23*, 205103. [CrossRef]
50. Nasution, E.Y.; Ahab, A.; Nuryadin, B.W.; Haryanto, F.; Arif, I.; Iskandar, F. Synthesis of gadolinium carbonate-conjugated-poly(ethylene)glycol ($Gd_2(CO_3)_3$@PEG) particles via a modified solvothermal method. *AIP Conf. Proc.* **2016**, *1710*, 030001–030007.

© 2019 by the authors. Licensee MDPI, Basel, Switzerland. This article is an open access article distributed under the terms and conditions of the Creative Commons Attribution (CC BY) license (http://creativecommons.org/licenses/by/4.0/).